

See discussions, stats, and author profiles for this publication at: <https://www.researchgate.net/publication/231376411>

Design and Packaging of Microreactors for High Pressure and High Temperature Applications

ARTICLE *in* INDUSTRIAL & ENGINEERING CHEMISTRY RESEARCH · OCTOBER 2010

Impact Factor: 2.59 · DOI: 10.1021/ie101346u

CITATIONS

52

READS

110

5 AUTHORS, INCLUDING:



Samuel Marre

Institut de Chimie de la matière condensée...

60 PUBLICATIONS 792 CITATIONS

[SEE PROFILE](#)



Andrea Adamo

Massachusetts Institute of Technology

19 PUBLICATIONS 242 CITATIONS

[SEE PROFILE](#)



Soubir Basak

SunEdison

15 PUBLICATIONS 264 CITATIONS

[SEE PROFILE](#)



Cyril Aymonier

French National Centre for Scientific Resea...

137 PUBLICATIONS 2,146 CITATIONS

[SEE PROFILE](#)

Design and Packaging of Microreactors for High Pressure and High Temperature Applications

Samuel Marre,^{†,‡,§} Andrea Adamo,^{†,§} Soubir Basak,[†] Cyril Aymonier,[‡] and Klavs F. Jensen*,[†]

Chemical Engineering Department, Massachusetts Institute of Technology, 77 Massachusetts Avenue, Cambridge, Massachusetts 02139, United States, and CNRS, Université de Bordeaux, ICMCB, 87 Avenue du Dr A. Schweitzer, F-33608 Pessac Cedex, France

The development of chemically compatible microsystems that can operate across expanded process conditions, such as high pressures (HP) and high temperatures (HT), is of great interest for many applications, including high pressure chemistry and hydrothermal and supercritical fluid processes. We present a methodology for the successful design and use of HP/HT microsystems. Key parameters for the fabrication of microreactors and modular fluidic packaging able to withstand severe pressure and temperature conditions (30 MPa, 400 °C) are described. Applications of these HP/HT plug and play microsystems are illustrated with examples, including multiphase flow visualization through the transition of liquid–liquid immiscible hexane–water segmented flow to homogeneous supercritical flow, on chip supercritical water oxidation, and synthesis of iron oxide nanoparticles.

Introduction

Chemical synthesis applications have increasingly been adapted to microfluidic systems to take advantage of miniaturization benefits such as low reagent consumption, fast screening, handling of highly reactive chemistry, and expanded operating regimes.^{1–13} Microreactors generally consist of patterned microchannels ranging from tens to hundreds of micrometers, etched or molded in a substrate, and sealed by bonding an additional substrate layer on the top. Microfluidic systems made of polymers, such as poly(dimethyl siloxane) (PDMS), are generally limited to conditions close to ambient temperature and atmospheric pressure.^{8,9,14} However, there is increasing interest in exploiting advantages of microfluidics for high pressure (HP) and high temperature (HT) applications.^{15–19}

Over the last two decades, microreactors that can withstand high pressure and high temperature have been fabricated in different substrates. For instance, metal microreactors are fabricated using laser ablation or EDM technique (electrical discharge machining), for applications in chemistry,⁶ such as in direct fluorination reactions,^{20,21} or for materials synthesis.²² Such metal microreactors are advantageous for processes involving high heat load and toxic chemicals due to good chemical compatibility and thermal resistance. Ceramics microreactors have been realized with molding techniques^{23,24} and are typically used for extremely high temperature processes (i.e., $T > 800$ °C) such as hydrogen production from continuous reforming of propane,^{23,25} catalyzed gas-phase reactions,²⁶ or nanomaterials synthesis.²⁷ Microreactors made of metal or ceramic can be fabricated without any clean room facilities, but the feature resolution of the design is restricted to several tens of micrometers due to the limitations of the available micro-machining tools. Microreactors made of silicon provide additional design options with well-developed microfabrication techniques, such as photolithography, and have excellent heat transfer characteristics, making them ideal candidates for HT processes, such as fuel conversion.^{8,28–30}

* To whom correspondence should be addressed. E-mail: kfjensen@mit.edu.

† Massachusetts Institute of Technology.

‡ Université de Bordeaux.

§ These two authors have contributed equally to this work.

Glass/glass microreactors are typically fabricated through HF or BOE (buffer oxide etchant) etching of either borosilicate^{31,32} or soda-lime glasses^{33,34} with subsequent thermal bonding. They have the advantage over previously mentioned microreactors in offering easy optical access, which provides the opportunity for implementing a wide range of *in situ* characterization techniques.³ Although high pressures can be reached using these microreactors,³⁵ the poor heat transfer of glass could impede fast temperature transitions and lead to generation of temperature gradients. Silicon/Pyrex microreactors, fabricated through silicon etching followed by bonding to Pyrex, have the advantage of allowing a very good thermal control, good chemical compatibility, and the possibility to reach high pressures, while keeping the advantage of an easy optical access through the Pyrex side. However, HP/HT applications of silicon/Pyrex microreactors have been limited by inadequate packaging schemes. The examples of HP/HT systems reported in the literature so far show an increased attention to expanded operating conditions, but these conditions are still somewhat limited either to high pressures or to high temperatures. For instance, Trachsel et al. and Murphy et al.^{15,36} have developed solder-based connected microsystems enabling work up to 14 MPa at 80 °C, while Tiggelaar et al. used epoxy gluing of fused silica tubing to glass microchips enabling work up to 40 MPa at 10 °C (or 15 MPa at 100 °C).³⁵ On the other hand, the connector developed by Pattekar et al. can reach 275 °C but withstand a limited pressure of 2.1 MPa.³⁷

In this work, we expand the operating conditions, reaching up to 30 MPa at 400 °C with a packaging that allows easy interchange of reactors and simplified experimental procedures. This is accomplished by a change in the paradigm: the requirements for high temperature and high pressure packaging are decoupled by having the connections between the chip and the external world on a mild temperature area of the chip ($RT < T < 250$ °C) where adequately designed compression parts can handle the high pressure. Another portion of the chip is heated up to the desired operating conditions (up to 500 °C, depending on pressure). The packaging scheme enables plug and play of reactors with different designs. The developed microreactor assembly is demonstrated for scientifically relevant HP/HT applications: first, investigation of phase diagrams

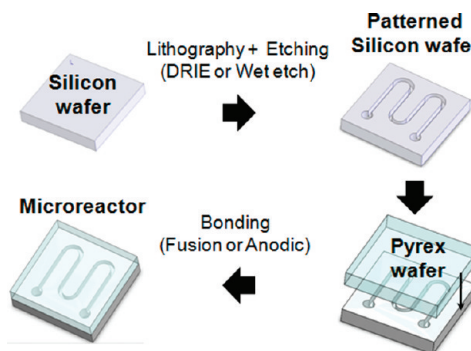


Figure 1. Schematic view of the microfabrication process.

through flow visualization of the transition to the supercritical homogeneous phase of a previously immiscible hexane/water flow by control of temperature and pressure; second, chemistry at high pressure and temperature with the supercritical water oxidation of methanol and phenol by H_2O_2 at conditions up to 25 MPa and 400 °C; third, synthesis of magnetic iron oxide nanoparticles in liquid toluene at 300 °C and 10 MPa.

General Strategy for Silicon–Pyrex Microreactor Fabrication

Microreactors made of silicon/Pyrex can be built with several standard silicon microfabrication techniques, depending on (i) the available equipment, (ii) the precision required for the design of the microscale features, and (iii) the required shapes of the channels. The conventional approach is detailed in Figure 1, starting from the patterning of a silicon wafer through both lithography and etching steps, followed by the covalent bonding of a Pyrex wafer to seal the channels. This latter step can be achieved through either fusion or anodic bonding process.^{38,39} However, deformation of Pyrex during fusion bonding ($T \sim 600$ °C) can possibly lead to channel obstruction when shallow or wide channels are considered. In contrast, anodic bonding process is done at temperatures far below the glass transition temperature of Pyrex ($T < 450$ °C). It ensures the absence of deformation, as well as a perfect sealing of the channel, while providing a pressure resistance bonding through the creation of covalent bonds.³⁹

The etching step can be achieved through different isotropic or anisotropic methods, either in wet or in dry etching modes, leading to a succession of channels (Figure 2a), whose shapes depend on the etching methods. Wet etching techniques include anisotropic KOH or TMAH (tetramethylammonium hydroxide) etching of silicon, leading to triangular or trapezoidal channels (Figure 2b)^{40–44} and isotropic etching with the HNA method (HF + nitric acid + acetic acid), leading to semicircular channels (Figure 2c).^{45,46} Dry etching techniques include well-developed anisotropic deep reactive ion etching (DRIE). Compared to the other silicon etching techniques, DRIE, coupled to lithography, provides an advanced control of the features, down to 1–2 μm in lateral resolution and leads to channels with straight side walls up to several hundreds of micrometers in depth (Figure 2d).

Design Considerations for HP/HT Microreactors

Microreactors for HP/HT applications require adequate sizing of channel dimensions (Figure 2b, 2c, and 2d) to ensure they are able to withstand the mechanical loads determined by the pressure and the thermal load. For practical purposes, a first-guess sizing of the reactor can be done with a structural model with a simplified loading condition and simplified structural

scheme. We have followed such an approach to help assignment of dimensions to the reactors which were built and tested. A more comprehensive analysis has also been carried out with finite element modeling (FEM) to gain better understanding of the weakness of the reactors in high pressure operations.

In general, the design problem involves sizing the various parts of a reactor so that, under operating conditions, failure does not occur. To this purpose, the stresses in the material have to be smaller than a limiting stress condition that determines failure. Silicon and Pyrex exhibit brittle fracture; therefore, we can use the method of the maximum normal stress, or Rankin criterion, as a failure criterion. According to this criterion, all the principal stresses⁴⁷ have to be greater than the ultimate compressive strength of the material (usually compressive stresses have negative values) and smaller than the ultimate tensile strength of the material (usually tensile stresses have positive values). Brittle materials exhibit a sudden rupture after an essentially elastic deformation without yield. The value of stress in the material at rupture is called ultimate strength. Ductile materials, upon increase of applied stress, show first an elastic behavior, and then, after yield, show a plastic deformation until rupture.

Simplified Structural Model. A first-guess sizing of the microreactor design parameters can be done using a simplified structural model. Assuming that the cross-section of a microreactor can be regarded as a periodic structure (Figure 2a), only one repeated element centered on a channel needs to be considered (Figure 2b, 2c, and 2d). To ensure the strength of the silicon component, the maximum tensile stress present in the silicon (approximated by eq 1) has to be less than the ultimate tensile stress of silicon. In particular the bottom of the channel needs to have thicknesses ($t_s - d$), such that:

$$\sigma_{s,\max} = k_1 k_s \frac{pw_s^2}{2(t_s - d)^2} \leq \sigma_{s,u} \quad (1)$$

where $\sigma_{s,\max}$ is the maximum value of tensile stress in the bottom part of the silicon channel, $\sigma_{s,u}$ is the ultimate tensile stress of silicon at the working temperature ($\sigma_{s,u} \sim 1$ GPa at 25 °C and decreases to $\sigma_{s,u} \sim 300$ MPa at 500 °C⁴⁸), and p is the pressure inside the channels. k_1 is a constant coefficient that takes into account the stress concentration at the edges due to the deep beam approximation (values should be between 5 and 10).⁴⁹ k_s is a safety factor, taking into account that (i) there are stress components that are being neglected (shear stresses and stresses in planes other than the cross-section plane are not considered; stresses induced by thermal loading are also neglected), (ii) stress concentration occurs at the corners, and (iii) failure of the chips is likely to be caused by stress concentration at microcracks or imperfections in the silicon wafer (a suggested value for k_s is 10). Equation 1 is dimensionally consistent, assuming the unit depth of the section.

Additionally, to ensure a sufficient bonding surface between Pyrex and silicon, we have experimentally determined that the general relation should be verified to prevent failure:

$$z \geq w_s \quad (2)$$

Since Pyrex and silicon have different elastic moduli, it is also proposed to select the thicknesses of the two wafers so that their ratio is close to the inverse ratio of their elastic moduli, in order to ensure that both collaborate in absorbing the loads:

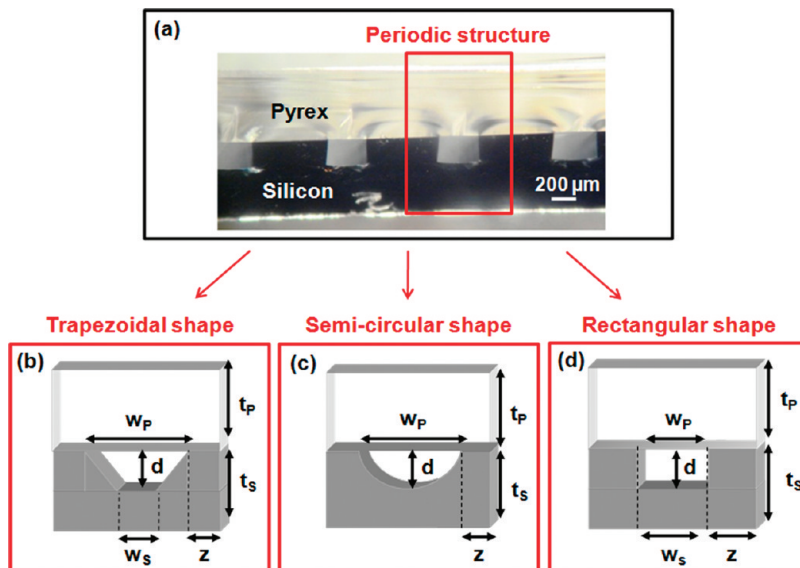


Figure 2. (a) Optical microscopy image of a microreactor cross-section with rectangular shape channels. (b–d) Scheme of the cross-section of a single microchannel with relevant parameters for the design for trapezoidal, semicircular, and rectangular shape channels, respectively. (Depth d , width w_p for the Pyrex side, and w_s for the silicon side, distance between channels $2z$, thickness of the silicon t_s and the Pyrex t_p wafer).

$$\frac{t_p}{t_s} \approx \frac{E_s}{E_p} \quad (3)$$

A similar expression to eq 1 can be used for the Pyrex:

$$\sigma_{p,\max} = k_1 k_s \frac{p w_p^2}{2 t_p^2} \leq \sigma_{p,u} \quad (4)$$

where $\sigma_{p,\max}$ and $\sigma_{p,u}$ are the maximum value of tensile stress and the ultimate tensile stress in the Pyrex, respectively. Uncertainty in the estimation of $\sigma_{p,u}$ could make this formula difficult to use (although typical values from literature are in the range 20–5000 MPa, we can assume $\sigma_{p,u} \sim 280$ MPa, corresponding to average quality borosilicate glasses). Nevertheless, we have found that eq 1 coupled to conditions 2 and 3 provide directions in reactor sizing.

The above analysis is valid for channels with rectangular and trapezoidal cross-sections. While in the first case w_s and w_p are equivalent, in the case of trapezoidal cross-sections, w_s should correspond to the width of the flat bottom part of the channel, while w_p should be the entire width. As shown later with the FE analysis, the stress concentration at the corners suggests that channels with a semicircular cross-section (obtained from using isotropic etching of silicon–HNA method) could have a better performance in high pressure/high temperature situations.

By applying this simplified structural model to microreactor design, we can predict using eqs 1 and 4 (assuming conditions 2 and 3 are fulfilled) whether the microreactor with rectangular cross-section channels will handle a certain amount of pressure at room temperature. For instance, Table 1 shows two examples of prediction when 20 or 45 MPa are applied inside two different rectangular cross-section channel microreactors D1 and D2 at 25 °C.

The results show that the obtained values of $\sigma_{s,\max}$ and $\sigma_{p,\max}$ are far below the ultimate tensile strength of both silicon and Pyrex when a pressure of 45 MPa is applied in design D1 channels, meaning that the microreactor should not break. However, in the case of $p = 20$ MPa applied within design D2 channels, both $\sigma_{s,\max}$ and $\sigma_{p,\max}$ are on the order of magnitude of $\sigma_{s,u}$ and $\sigma_{p,u}$ (1 GPa and 280 MPa, respectively, at 25 °C),

Table 1. Main Characteristics of Two Pressurized Microchannel Designs D1 and D2 (e.g., w_p , w_s , t_p , t_s , d , $2z$, and applied pressures inside the channel (AP)) and Resulting Maximum Tensile Strength for Both Silicon ($\sigma_{s,\max}$) and Pyrex ($\sigma_{p,\max}$) Obtained from the Application of the Simplified Structural Model for Given k_1 and k_s Values

design	k_s	k_1	$w_p = w_s$ (μm)	t_p (mm)	t_s (mm)	d (μm)	$2z$ (μm)	AP (MPa)	$\sigma_{s,\max}$ (MPa)	$\sigma_{p,\max}$ (MPa)
D1	10	10	200	1.5	1	150	200	45	124	40
D2	10	10	400	0.76	0.65	200	400	20	790	277

meaning that the maximum working pressure allowed in this type of channel is reached and the integrity of the microreactor could be compromised.

Finite Element Modeling. For the selected microreactor designs (D1 and D2) we carried out a more detailed analysis of the stress distribution with a finite element model through the use of the plain strain static solver of COMSOL Femlab 3.1. The finite element simulation allows us to explore the mechanical behavior of the chip under more realistic loading and geometry conditions. Figure 3A and 3B shows a plot of the maximum (top) and minimum (bottom) value of the principal stresses in the reactor for four different designs, whose main characteristics are summarized in Table 2 (D1 and D2, Figure 3A, presented in Table 1, and C1 and C2, Figure 3B, which have semicircular cross-sections designs with size and loading conditions comparable to D1 and D2).

Since our purpose is to identify whether the microreactor will fail at the operating pressures, following the Rankine failure criterium, the maximum principal stress in Figure 3A and 3B (a tensile stress) has to be less than the ultimate tensile strength of the material (for both material) and the minimum principal stress has to be greater than the ultimate compressive strength of the material.

An analysis of Figure 3A and 3B shows that significant stress concentration occurs in the internal corners of the channel cross-section and the stress values rapidly decrease away from the corners. Since the sharp stress concentration is also at the corners of the Pyrex/silicon interface, it is important to use Pyrex with a very good quality surface, as any microscratch provides the initial locus for failure. As a matter of fact, glass-based products fabricated with a high quality external surface finishing typically exhibit ultimate

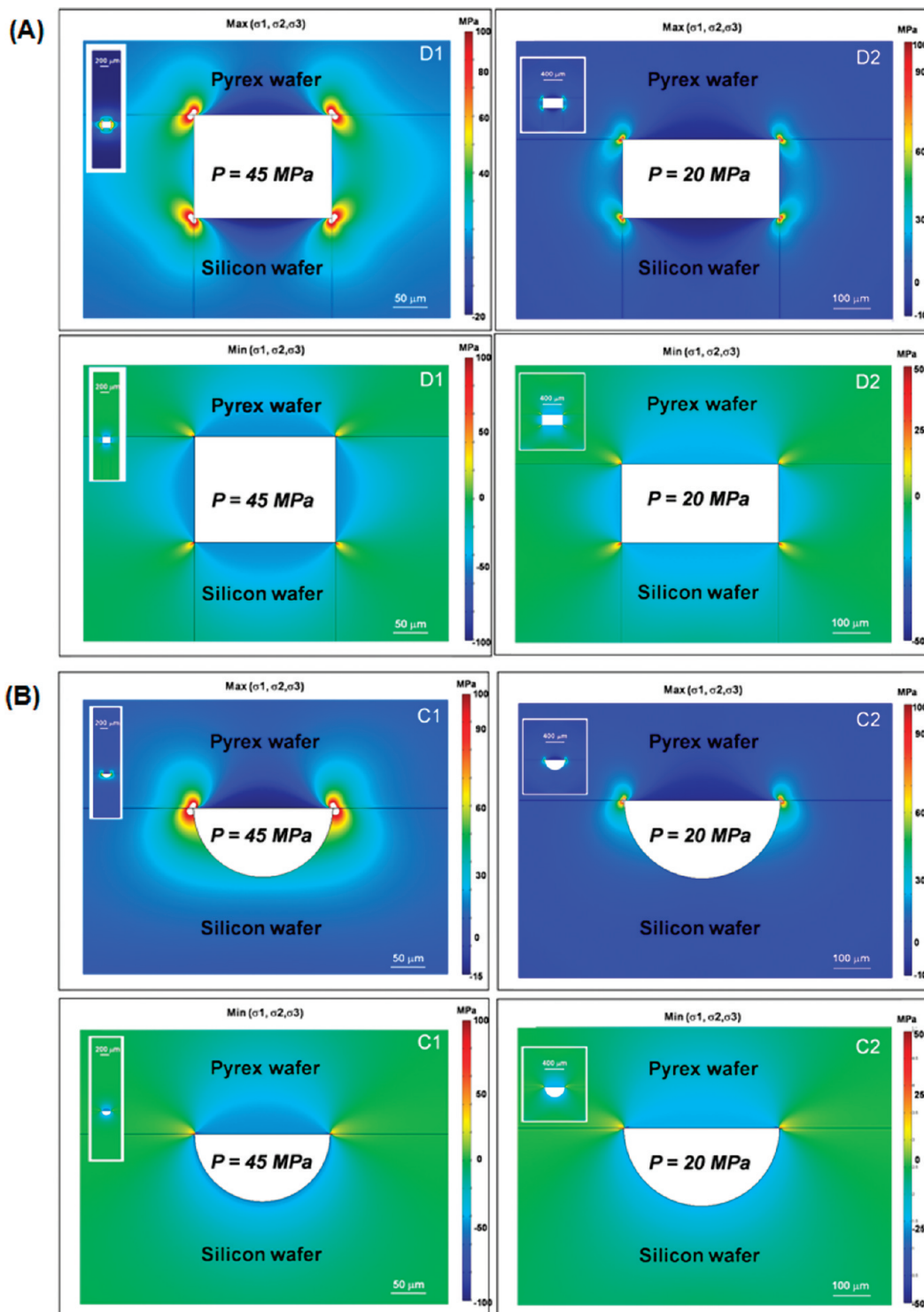


Figure 3. (A) 2-D Finite Elements Analysis (COMSOL Femlab 3.1) of the cross-section of a periodic element of two microreactor designs with rectangular cross-section. In all cases, the white spots outside the color bar range at the corners are where the principal stresses exceed the maximum of the scale bar (in all cases by less than 8% of the scale bar maximum). Details of the geometries are presented in Table 1. Top figures show the maximum value of the principal stresses at each point; bottom figures show the minimum value of the principal stresses at each point. For the simulation we used $E_{\text{silicon}} = 131 \text{ GPa}$, $E_{\text{pyrex}} = 64 \text{ GPa}$, Poisson's coefficients: $\nu_{\text{silicon}} = 0.5$, $\nu_{\text{pyrex}} = 0.2$. (B) 2-D Finite Elements Analysis (COMSOL Femlab 3.1) of the cross-section of a periodic element of two microreactor designs with semicircular cross-section. In all cases, the white spots outside the color bar range at the corners are where the principal stresses exceed the maximum of the scale bar (in all cases by less than 8% of the scale bar maximum). Details of the geometries are presented in Table 1. Top figures show the maximum value of the principal stresses at each point. Bottom figures show the minimum value of the principal stresses at each point. For the simulation we used $E_{\text{silicon}} = 131 \text{ GPa}$, $E_{\text{pyrex}} = 64 \text{ GPa}$, $\nu_{\text{silicon}} = 0.5$, $\nu_{\text{pyrex}} = 0.2$.

tensile stress orders of a magnitude greater than what is usually reported (in the simplified structural model, we used $\sigma_{p,u} \sim 280 \text{ MPa}$, corresponding to average quality borosilicate glasses; however, optical fibers can exhibit an ultimate tensile stress $\sim 5 \text{ GPa}$).⁵⁰ We used a Pyrex wafer with scratch/dig = 60/40 and surface finish $< 20 \text{ Å}$; it can be speculated that

better surfaces may give better performance than described here but at a significant increase in cost of supplies. Pyrex exhibits the smallest ultimate tensile strength and therefore provides more stringent conditions on the design.

Considering semicircular shape channels (designs C1 and C2, Figures 3B) with equal w_p as designs D1 and D2, respectively,

Table 2. General Characteristics of the Four Microchannel Designs: Cross-Section Shape, w_p , w_s , t_p , t_s , d , z , Working Pressure Inside the Channel (WP)

design	cross-section	w_p (μm)	w_s (μm)	t_p (mm)	t_s (mm)	d (μm)	z (μm)	WP (MPa)
D1	rectangular	200	200	1.5	1	150	200	45
D2	rectangular	400	400	0.76	0.65	200	400	20
C1	semicircular	200	—	1.5	1	150	200	45
C2	semicircular	400	—	0.76	0.65	200	400	20

the results show stress levels comparable with D1 and D2 with the extra advantage of the reduction of stress concentration points. This could provide a better performance of this section with respect to the rectangular one; however, this potential advantage would come at the cost of reduction of the channel cross-section (for assigned w_p) since w_p is a critical parameter for Pyrex performance. The potential advantages of this cross-section could be further reduced by the stress concentration occurring at the internal corners between silicon and Pyrex, and Pyrex is the material with the weaker ultimate tensile strength. We limited our simulations to rectangular and semicircular cross-section channels, since trapezoidal channels lead to similar results as rectangular channels.

On the basis of the insight gained by the above two analyses, we have built and used HP/HT microreactors. In this study, the microchannels were patterned on a silicon wafer ($\phi = 15 \text{ cm}$, $0.65 \text{ mm} < t_s < 1 \text{ mm}$) with DRIE,⁵¹ leading to rectangular shape channels. Once the channels were patterned on the silicon wafer, an oxide layer ($0.5 \mu\text{m}$) was grown through wet oxidation for improved chemical compatibility, and a Pyrex wafer ($0.76 \text{ mm} < t_p < 1.5 \text{ mm}$) was anodically bonded on the top.

The general layout (Figure 4) consists of a reaction zone (heated up to 450°C) and an injection zone (kept at lower temperature) separated by an insulation area where the silicon is etched away to minimize heat conduction. The channels are patterned with photolithography, enabling easy realization of different channel layouts.

Figure 4 shows different microreactor designs for various targeted applications. A single 1.5 m long channel microreactor for nanoparticle synthesis and supercritical water oxidation is shown in Figure 4a, and a microreactor equipped with shallow side channels (width = $100 \times$ depth = $50 \mu\text{m}$) for the continuous feed of additional reagents to a main channel ($400 \times 200 \mu\text{m}$) is shown in Figure 4b. Other designs include a microreactor for studying coflowing fluids ($200 \times 150 \mu\text{m}$) (Figure 4c) and a microreactor for generating high pressure two-dimensional jets (nozzle: $20 \times 50 \mu\text{m}$) (Figure 4d). In all cases, the position of the inlet/outlet holes are kept constant, to ensure a standard packaging (modular fluidic connection and heating chuck) can be used for all microreactors.

Since silicon and Pyrex exhibit close thermal expansion coefficients values, temperature does not add significant additional stress within materials as long as either the high temperature or the cold temperature area is considered. However, the modification of the maximal tensile strength of the materials with the temperature may become significant at high temperatures. Although borosilicate glasses retain their mechanical strength over a range of temperature, they will deform at temperatures approaching their strain point (e.g., 510°C for Pyrex). Additionally, the temperature effect becomes relevant in the insulation zone, which experiences a thermal gradient. Such a large thermal gradient introduces considerable mechanical stresses within the reactor materials. Stresses tend to concentrate near sharp corners so the region separating two temperature zones in the reactor should be designed to minimize the occurrence of such features. An estimate of the stress field

in the device (not shown here) was calculated using a 2-D finite element analysis (COMSOL Femlab 3.1), demonstrating that eliminating sharp corners in the region between temperature sections greatly reduces thermally induced stresses on the device.⁵²

Packaging of Microreactors

Conventional connection methods are divided in two main families. (1) Permanent integrated connections, including epoxy gluing,^{35,37} metal soldering,^{15,36} glass brazing,^{53,54} or anodic bonding of Kovar tubes to glass.⁵⁵ These fluidic connections are reported to stand up to 17 MPa or more with particular designs. However, these techniques generally require complicated microfabrication procedures to optimize the connection strength, are not versatile in term of chemical compatibility, and are not reversible. (2) Nonpermanent modular connections such as commercial microfluidic interface assemblies that can withstand 10 MPa ^{56–58} or compression sealing with rubber O-rings.¹⁸ For this study, fluidic connections based on this latter option are developed, since they are less time-consuming in term of fabrication and, more importantly, provide the opportunity for easy interchange of microreactors.

HT/HP performance and modular design have been achieved by decoupling the HP and HT problems. It is usually difficult to find materials resisting HP and HT at the same time; therefore, we have created a “cold zone” where we are able to use a compression scheme for the package handling HP at mild temperature ($T < 250^\circ\text{C}$). Another portion of the chip is heated, creating a “hot zone” where the desired operating conditions are thus reached.

The compression chuck consists of two stainless steel parts compressing the microreactor (Figure 5). The bottom one is dedicated to the connection of tubing with conventional Upchurch 10-32 ports (Figure 5a-1). It can be cooled through holes designed for a coolant supply (Figure 5a-2). The upper part (Figure 5a-3) aims at compressing the microreactor against O-rings (Figure 5a-4) and holding pressure. The upper part is equipped with a window, allowing visualization of the microreactor inlet after injection of the fluids. In order to ensure good homogeneity in the compression, while keeping the advantages of the optical access, an additional Pyrex part (thickness range is $6\text{--}12 \text{ mm}$) is placed in between the microreactor and the upper part (Figure 5a-5).

There are several O-rings materials that can be chosen (Viton, PTFE, Kalrez, or silicone) based on the process parameters such as pressure, working temperature (in the inlet area), and chemicals in use. The hardness of the O-rings and the design of the grooves are key parameters when high pressures are considered.⁵⁹ The typical hardness range for successful sealing at pressures above 15 MPa is $75\text{--}90$ (hardness shore A). Figure 5b presents an image of the [microreactor–compression part] assembly.

Design of the Modular Compression Package. The design of the compression parts for high pressure applications was challenging due to the magnitude of the pressures involved and the brittle nature of silicon/Pyrex microfluidic devices. Moreover, the high temperature applications required that materials withstand a thermal load. Attention was given to identify the deformation of the compression parts when loaded, which was a key issue for a successful use of the packaging technique.

Deformation of the compression parts hampers successful sealing. The subsequent overtightening to counteract the effect of the deformation not only deforms the part even more but also determines a load concentration on the edges of the

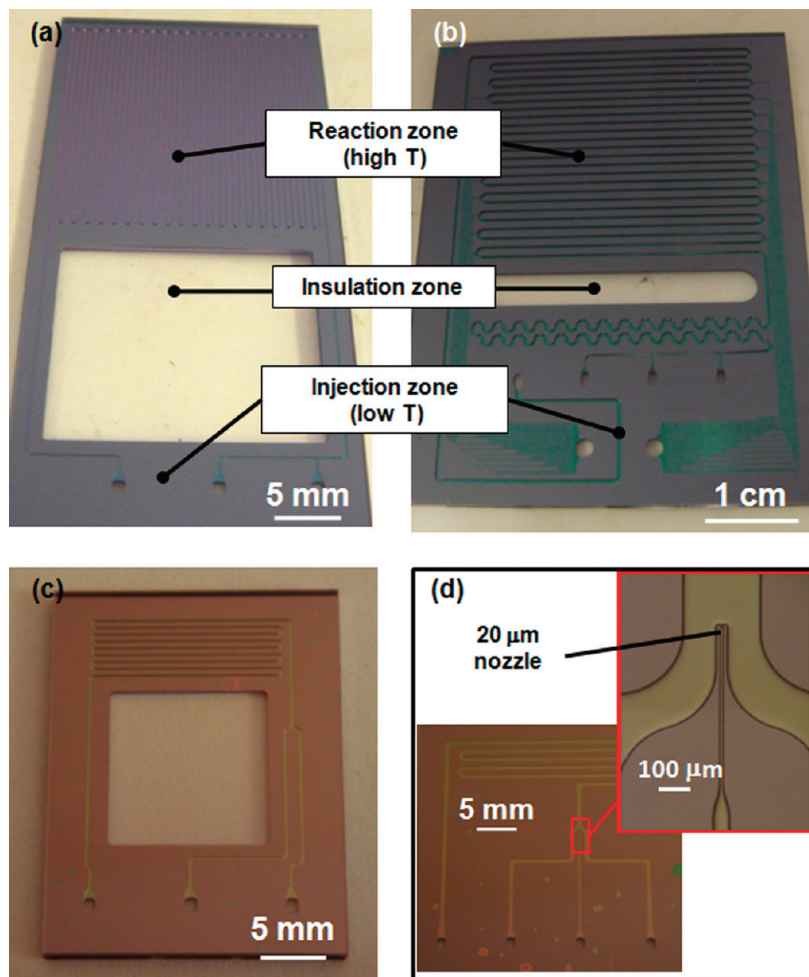


Figure 4. Examples of HP/HT microreactor designs. (a) Single channel microreactor, (b) microreactor equipped with shallow side channels for the continuous feed of additional reagents to a main deep channel, (c) microreactor used to observe coflowing fluids, and (d) microreactor used to generate high pressure two-dimensional jets.

microreactor and leads to fracture. Therefore, if compression parts are adequately stiff, under working conditions, the microreactor can be regarded as compressed between two parallel rigid plates and correct sealing is achieved.

A compression part can be regarded as rigid if, under operation conditions, the maximum deformation of the microreactor (*d*, Figure 6) is on the order of a few micrometers *d* can be calculated as:³⁶

$$d = d_1 + d_2$$

$$d_1 = \frac{F\epsilon l^2}{8EJ}$$

$$d_2 = \frac{qc}{384EJ} \times (c^3 - 4lc^2 + 8l^3)$$

where *b* is the thickness of the cross-section of the area over which pressure is exerted, *c* is the width of the loaded area (*c* = 1, in this design), ϵ is the distance between the edge of the microreactor and the bolt, *E* is the elastic modulus of the material selected for the compression part, *d*₁ is the deformation due to force *F* applied by the bolts, *d*₂ is the contribution to the deformation due to the fluid pressure that acts as a distributed load onto the compression part, *h* is the thickness of the compression part, and *J* is the moment of inertia of the cross-section of the compression part (*J* = $h^3 \times b/12$). The force applied by the bolts (*F*) is equal to the load applied by the fluid

pressure in addition to the load required to deform the O-rings. In high pressure applications the latter is small with respect to the former and can be practically ignored. Therefore, $F = q \times c/2$ where *q* is the load per unit length applied by the microreactor onto the compression part. *q* can be estimated by $q = p \times b$, with *p* the fluid pressure.

For a specific application, a successful compression part can be designed by restricting *d* on the order of a few micrometers. If the condition is not satisfied, either *h* can be increased or the geometry of the microreactor can be changed in order to decrease the distance between the bolts of the compression part.

Design of the High Temperature Zone. Applications of the microsystems require both HP and HT conditions so the packaging scheme must allow for a temperature-controlled zone for the microreactor. The portion of the microreactor in which the reactions take place is contacted with a heated aluminum block, while the modular fluidic connection is cooled with a cooling flow. Cooling the fluidic interface has three advantages: (i) simplifying the packaging scheme, as the packaging challenge becomes only a HP problem since the HT handling is reduced; (ii) minimizing thermal expansion problems in the compression chuck; (iii) quenching of chemical reactions within the micro-channel, which ensures good control of the reaction volume. The hot and cold zones are thermally separated by an insulation area designed in the microreactor by etching away silicon to reduce heat transfer (Figure 7). The aluminum block is equipped with heating cartridges and thermocouples. A graphite gasket

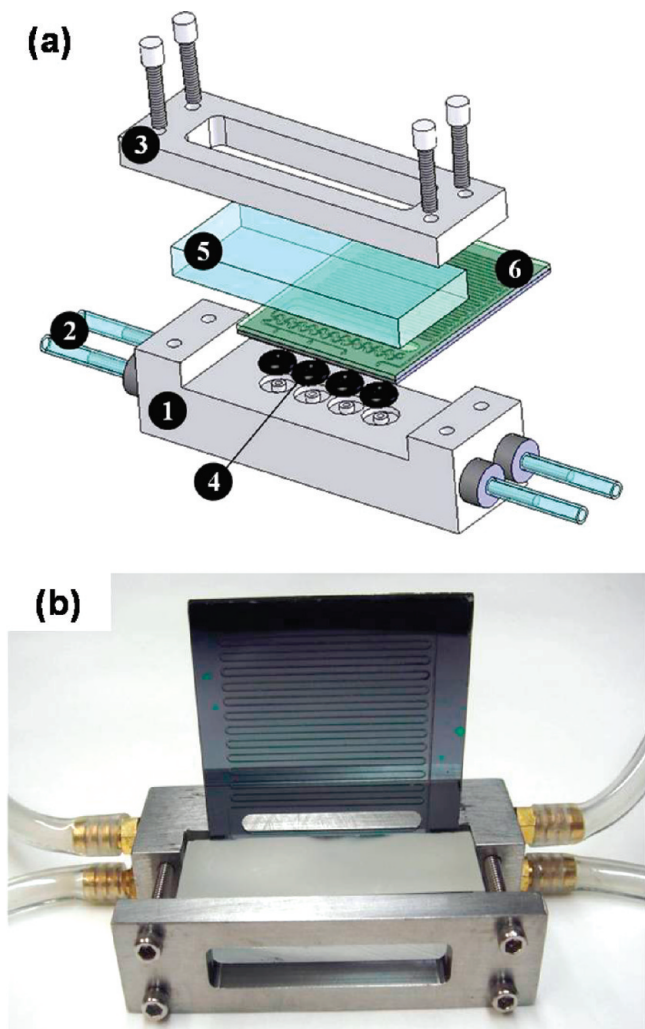


Figure 5. (a) Scheme of a high pressure microsystem assembly: (1) compression part, (bottom) with modular fluidics inlet/outlet ports, (2) cooling fluid pathway, (3) compression part (top) (4) O-rings and grooves, (5) Pyrex plate for optical access, (6) microreactor. (b) Image of the final assembly.

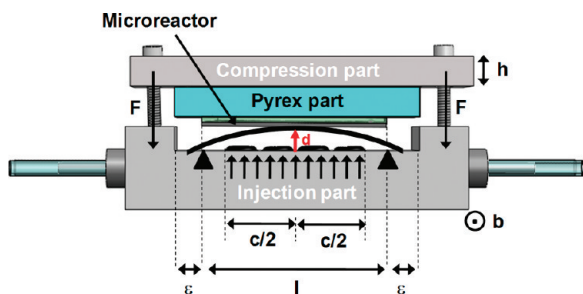


Figure 6. Scheme of the compression part under loading conditions.

compressed between the heater block and microreactor improves thermal conduction between the two parts.

Uniform temperature distribution was achieved for the heated section. However, depending on the position of the aluminum heating block, it is also possible to generate a thermal gradient along the microreactor, or to create working zones with different temperatures according to process requirements. The final assembly of the modular compression fittings and the heating block leads to a HP/HT plug and play microsystem in which the microreactors can be easily exchanged.

Performance Testing of the Microsystem Assembly. Several designs with different channel sizes and substrate thick-

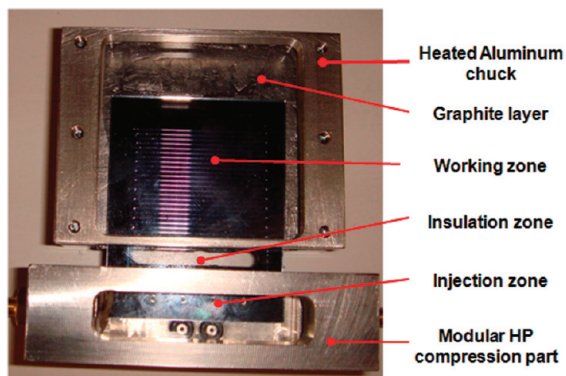


Figure 7. Microsystem assembly for HP/HT applications.

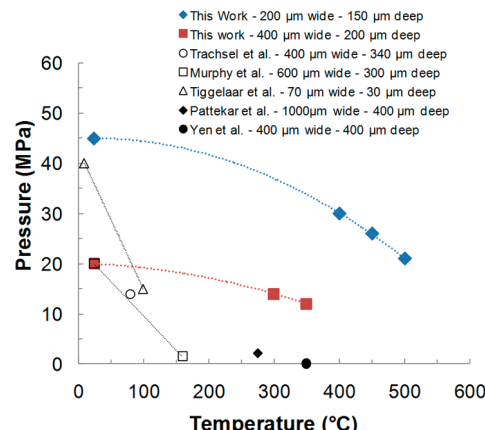


Figure 8. Maximal operating conditions tested for the microsystem assemblies for which no failures were noticed and comparison with available data from Trachsel et al.,¹⁵ Murphy et al.,³⁶ Tiggelaar et al.,³⁵ Pattekar et al.,³⁷ and Yen et al.⁵³

nesses were experimentally tested at different operating conditions. Failure of the microreactors was not always repeatable, and this observation is consistent with both silicon and Pyrex being brittle materials. Their fracture is determined by micro-crack growth where stress concentration occurs.⁶⁰

Mechanical stress testing was first performed on the compression part itself, applying pressures up to 50 MPa through the Upchurch ports against a Pyrex plate (0.5 in. thick) placed in the compression part (similar to Figure 5a), without mounting any microreactor.

In the second step, the microsystems were tested at room temperature by pressurizing the microreactors with liquid CO₂ at constant flow rate (100 $\mu\text{L min}^{-1}$) using a high pressure pump (Teledyne Isco, Model 260D). While no failure was noticed for design D₁ up to a pressure of 45 MPa, design D₂ showed reproducible failure for $p > 20$ MPa from the Pyrex breakage (Figure 8). These observations, compared to the results obtained with the simplified structural model, suggest that a safety factor (k_s) in the design stage of about 10 is appropriate. A failure of the anodic bond between Pyrex and silicon was never observed during the tests; however, failure of the Pyrex just above the interface between the two materials was observed several times, likely due to cracks propagating from the corners of the channel.

The final step of the mechanical testing consisted of heating the reaction zone of the microreactor ($T > 350$ °C) while under high pressure conditions (up to 30 MPa). The same experiments were performed under both pressure and temperature conditions using the microsystem previously described (Figure 7). In these experiments, the microreactors with the design D₁ withstood

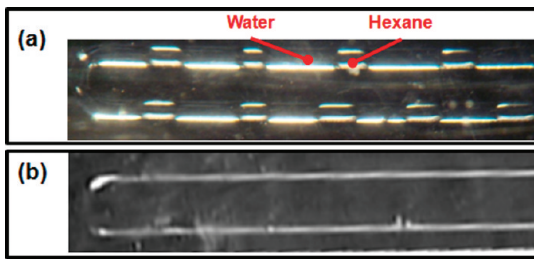


Figure 9. Hexane–water flows generated in a HP/HT microsystem at different conditions: (a) segmented liquid–liquid flow at $T = 25\text{ }^{\circ}\text{C}$ and $p = 0.1\text{ MPa}$. (b) Homogeneous supercritical flow at $390\text{ }^{\circ}\text{C}$ and $p = 23\text{ MPa}$.

conditions up to $450\text{ }^{\circ}\text{C}$ and 25 MPa without failure, and in some cases, microreactors have shown no failure up to $500\text{ }^{\circ}\text{C}$ and 30 MPa . For design D₂, failures occurred generally close to 12 MPa for a temperature of $350\text{ }^{\circ}\text{C}$. Similar to room temperature experiments, the Pyrex breaks first at high temperature.

As shown in Figure 8, the assemblies [packaging + microreactors] developed and used in this study exhibit much wider operating conditions. The critical point is the ability to use both high pressure and high temperature at the same time compared to previously developed microsystems restricted to either high pressure/low temperature or high temperature/low pressure applications. Additionally, our reversible packaging allows for faster mounting of microreactors.

As a general rule, it is advisable to use gentle rates of pressurization and heating for the successful use and (p, T) cycling of these devices, especially when very high pressures ($p > 20\text{ MPa}$) and temperatures ($T > 350\text{ }^{\circ}\text{C}$) are considered. Otherwise, although the packaging is not a problem, the microreactor's integrity could be compromised. For instance, a typical temperature ramp should be close to a few tens of $^{\circ}\text{C}$ per minute, while pressure can be increased a few MPa per minute.

Note that another parameter has to be taken into account: the thermal gradient per length (ΔT_1 in $^{\circ}\text{C}/\text{mm}$) applied along the halo etch between the cold and the hot zones. Failures have been noticed in this area, independent of pressure conditions, when the values of ΔT_1 exceed $\sim 40\text{ }^{\circ}\text{C}/\text{mm}$. Therefore, halo etches with different lengths have to be designed depending on the applied temperature in the heated section of the microreactor.

Application of High Pressure/High Temperature Microsystems

Investigation of Phase Diagrams. The HP/HT microsystems were first used to optically characterize the transition of heterogeneous segmented liquid–liquid segmented flow to homogeneous supercritical fluids flow with a CCD camera. Water/hexane segmented slug flow was chosen as a model system to demonstrate the HP/HT capability of these microsystems. Starting from room temperature at 0.1 MPa (Figure 9a), the system was slowly pressurized with two HP syringe pumps (Isco 260D and Isco 100D) to 23 MPa , delivering hexane ($30\text{ }\mu\text{L min}^{-1}$) and water ($70\text{ }\mu\text{L min}^{-1}$), resulting in a $5/95$ molar ratio hexane to water. During that time, the temperature was increased to $390\text{ }^{\circ}\text{C}$. Considering the (p, T) diagram, these conditions are located above the critical point of water (i.e., $T_c = 374\text{ }^{\circ}\text{C}$, $p_c = 22.1\text{ MPa}$). Supercritical water exhibits a low dielectric constant ($\epsilon \sim 5.9$)⁶¹ similar to that of hexane at RT ($\epsilon \sim 2$), which makes it a nonpolar solvent. Therefore, hexane is miscible with supercritical water and the segmented flow turns

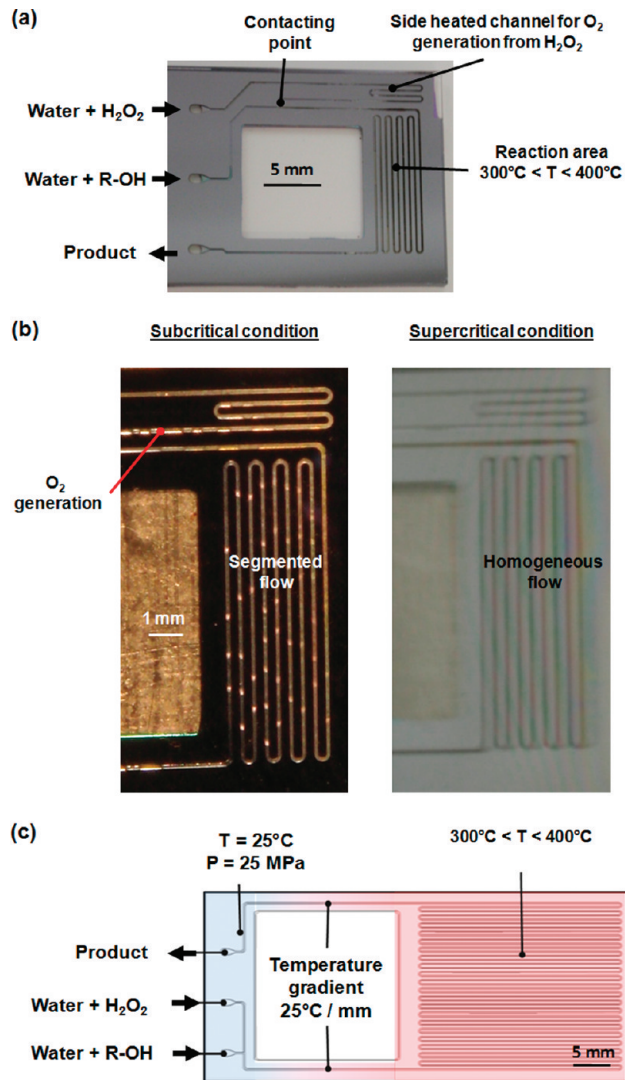


Figure 10. (a) Microsystem used for the μSCWO process visualization. (b) Optical flow characterization obtained for different conditions considering the sub- and supercritical water oxidation process of methanol by H_2O_2 . (c) Microsystem layout ($45\text{ }\mu\text{L}$ microreactor) for μSCWO conversion rate measurements of MeOH and PhOH.

homogeneous (Figure 9b). This first demonstration of HP/HT microreactor application highlights the potential of these microsystems for in situ investigations due to optical access through the Pyrex side, at conditions not reached previously.

Chemistry in Supercritical Water. The second application deals with chemical reactions in supercritical water (SCW). Numerous works have demonstrated potential applications for the oxidation of aqueous waste, for biomass valorization,⁶² and for materials recycling.⁶³ In addition, SCW is a potentially useful solvent⁶⁴ for organic chemistry^{61,65–68} and materials processing.^{69,70} The use of SCW in confined media opens avenues toward a large number of applications from green chemistry to geology, with the study of lithosphere fluids in microporous substrates. One can even envisage the development of pocket-size wastewater treatment factories for applications in long distance space exploration missions.⁷¹ However, the use of SCW implies high temperature and pressure conditions, which are particularly difficult to reach, especially within microsystems. To address this problem, we have designed microreactors able to handle $T = 450\text{ }^{\circ}\text{C}$ in the working zone and $p = 25\text{ MPa}$ without failures, conditions that are compatible with the use of SCW.

Table 3. Experimental Conditions Used for the μ SCWO of MeOH or PhOH with H₂O₂, Varying Temperature, Pressure, Residence Time (t_R), and Ratio of H₂O₂ to Alcohol (R)^a

alcohol/ tests	P (MPa)	T (°C)	R	t_R (s)	[R-OH] ₀ (wt %)	conversion (%)
PhOH-1	25	400	20/1	5	0.5	100
PhOH lit. ⁷³	24	400	5/1	30	0.5	52
	24	400	5/1	110	0.5	90
MeOH-1	20	300	7/1	2	15	36.5
MeOH-2	20	350	7/1	2	15	78.3
MeOH-3	25	380	7/1	2	15	87
MeOH lit. ⁷⁴	24.1	450	2.25/1	2.13	1.5	42
		460	2.25/1	2.01		80

^a The last column presents the conversion percentage of alcohol = $100 \times (1 - ([R\text{-OH}]/[R\text{-OH}]_0))$.

We focused our work on the sub- and supercritical water oxidation process (SCWO) in microreactors (μ SCWO) through the oxidation of methanol (MeOH) and phenol (PhOH) as model molecules by hydrogen peroxide, at conditions of $300 \text{ }^\circ\text{C} < T < 400 \text{ }^\circ\text{C}$ and $20 \text{ MPa} < p < 25 \text{ MPa}$.

Two microreactors were used, both equipped with two inlets and one outlet. For the first one, used to visualize flows (Figure 10a), a side channel was designed to preheat the oxidizing H₂O₂ solution (35 wt % in water), showing oxygen gas generation at subcritical conditions through the formation of a gas (O₂)–liquid (water) segmented flow (Figure 10b, left), whereas oxygen is fully dissolved in SCW, resulting in a homogeneous flow (Figure 10b, right). This flow was thereafter mixed with the MeOH or PhOH in water solution before entering the reaction zone (4.5 μL). The second microreactor (Figure 10c) allows the reactants to mix at room temperature before entering a longer reaction zone (45 μL) and was used to measure the conversion rate of MeOH and PhOH during μ SCWO, enabling longer residence times.

The general reaction equations are as follows:

For MeOH:



For PhOH:



The oxidation proceeds within seconds, taking advantage of the high surface to volume ratio in microchannels, leading to fast heat transfer. Therefore, we fixed the residence time to 2 s for the methanol solution and 5 s for the phenol solution.⁷² Four samples were collected (three for MeOH and one for PhOH), as summarized in Table 3, varying the temperature from subcritical conditions (300 and 350 °C) to supercritical condi-

tions (380 and 400 °C). Interestingly, the μ SCWO of PhOH and MeOH leads to higher conversion values compared to the results obtained in the literature in stainless steel pipes (Table 3).^{73,74}

For the PhOH oxidation, we worked in large excess ($R = 20/1$) of hydrogen peroxide to phenol, with a residence time of 5 s, resulting in typical flow rates: H₂O₂ (35 wt % in water) = 53 $\mu\text{L}/\text{min}$ and PhOH (0.5 wt % in water) = 37 $\mu\text{L}/\text{min}$. The collected product was analyzed with gas phase chromatography (Agilent Technology model 6890N) showing no remaining phenol in the studied conditions. When these results are compared to those from the literature, obtained under the same conditions except for a lower value of R (5/1), it is obvious that μ SCWO seems to allow higher yields in a shorter residence time. Indeed, μ SCWO results in PhOH conversion of 100% in 5 s, which value has to be compared with PhOH conversion of 52% and 90%, obtained for residence time of 30 and 110 s, respectively, reported in the literature.⁷³

Considering the MeOH oxidation, for a fixed value of R (7/1) at $t_R = 2$ s and $20 < p < 25 \text{ MPa}$ for T ranging from 300 to 380 °C, the conversion rate varies from 36.5% to 87%. This has to be compared with the conversion rates obtained in the literature under somewhat the same conditions ($t_R \sim 2$ s, $p = 24.1 \text{ MPa}$) except for a lower R (2.25/1) but much higher temperatures (450–460 °C) and a lower initial concentration of methanol (1.5%). For the data obtained under supercritical conditions ($T = 380 \text{ }^\circ\text{C}$), the conversion rate was equivalent to that reported in the literature in macroscale systems at 460 °C.

Several factors can generally account for the differences observed when dealing with conventional SCWO of PhOH or MeOH, which were carefully reported in a critical review of the subject.⁷⁵ Among these factors are mixing effect, preheating of H₂O₂, and reactor wall catalysis. In the μ SCWO of PhOH considered in this study, it is likely the large excess of H₂O₂ has greatly contributed to the increase in reaction kinetics and therefore the final yield of the PhOH conversion. This effect can also occur in the μ SCWO of MeOH ($R = 7/1$ in this study, compared to $R = 2.25/1$ in the literature), although it was reported that the influence of R for values beyond 2 was negligible.⁷⁵ Among the other factors responsible for the improvements of the degradation kinetics when using μ SCWO, we can make assumptions concerning the influence of the initial concentration of methanol. High initial methanol concentrations (used this study, e.g., wt% = 15%) generally exhibit higher apparent first-order constants by producing hot zones within the reactor and by decreasing induction time.⁷⁵ In our case, the hot zones are unlikely to happen, given the high heat transfer capability of the microreactor. However, this capability also allows for heating the flowing fluid much faster than macroscale

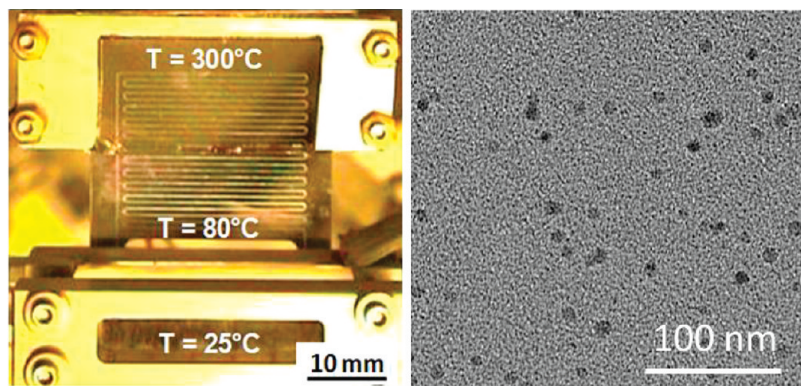


Figure 11. A 100 μL microreactor for the two-step on-chip synthesis of iron oxide NPs in liquid toluene at HP/HT conditions and a TEM image.

systems, therefore reducing considerably the induction time of the oxidation reaction. Once more, this demonstration highlights the high potential of such HP/HT microsystems for studying and improving chemical reactions under expanded conditions using continuous microscale processes.

Materials Synthesis. The synthesis of iron oxide nanoparticles (NPs) in a two-step process constitutes another example. The synthesis procedure is based on previous work in batch mode using high boiling point solvent systems.⁷⁶ Here, thanks to the ability to use HP/HT conditions within microreactors, we replaced these solvent systems with toluene, which is maintained as a liquid at 300 °C by applying pressure ($p = 10$ MPa). The general procedure consists of preparing two solutions of (i) iron pentacarbonyl ($\text{Fe}(\text{CO})_5$, 10 mM) in toluene, and (ii) oleic acid (30 mM) in toluene, which are thereafter loaded in separated high pressure pumps before being injected at equal flow rates (26 $\mu\text{L min}^{-1}$) into a 80 μL microreactor through two different inlets. By selectively heating only the top of the microreactor, an on-chip thermal gradient can be generated, which is used to create two temperature zones along the microreactor (Figure 11, left). The first one allows for a prereaction between the iron pentacarbonyl and the oleic acid, in order to form iron oleate in the temperature range 80–150 °C. The later thermal decomposition of the iron oleate in the high temperature area ($T = 300$ °C) leads to the nucleation of iron oxide NPs (Fe_3O_4). The total residence time was 1 min, leading to an average size of 8 nm for the NPs (Figure 11, right).

Through these first examples, we demonstrate the potential of microsystems for the study and development of applications at HP/HT, such as supercritical water or engineering fluids processes. Additional potential applications include other syntheses of nanomaterials such as quantum dots, as previously demonstrated,¹⁸ catalysts, or oxides (as exemplified in here), on account of the access to conditions not easily attained in bath mode.

Conclusion

A method for the successful design, packaging, and “plug and play” use of silicon/Pyrex microreactors for high pressure/high temperature applications is proposed. The designs were mechanically tested for operating conditions up to 400 °C and 25 MPa, and the use of the microreactors for three different applications involving supercritical water or pressurized liquid toluene was demonstrated.

The expansion of the temperature/pressure domain of the on-chip operating conditions will benefit research in several areas. For instance, the available conditions for chemical synthesis have been expanded relative to batch opening opportunities for new efficient reaction routes and use of supercritical solvents for chemical transformation and production of novel nanostructures. Moreover, these microsystems could also be used for fundamental phase diagram studies in various fluidic systems. Importantly, the methodology provides a flexible tool for scientists interested in mimicking the harsh temperature and pressure conditions of lithosphere fluids found underground at large depths.

Acknowledgment

The US National Science Foundation (CHE-0714189), the US Army Research Office through the Institute for Soldier Nanotechnology (DAAD-19-02-0002), the GIS “Advanced Materials in Aquitaine”, and the MIT-France program are gratefully acknowledged for financial support.

Literature Cited

- (1) Marre, S.; Jensen, K. F. Synthesis of Micro and nanoparticles in microfluidic systems. *Chem. Soc. Rev.* **2010**, *39*, 1183–1202.
- (2) Baxendale, I. R.; Deeley, J.; Griffiths-Jones, C. M.; Ley, S. V.; Saaby, S.; Tramner, G. K. A flow process for the multi-step synthesis of the alkaloid natural product oxomaritidine: a new paradigm for molecular assembly. *Chem. Commun.* **2006**, *(24)*, 2566–2568.
- (3) deMello, A. J. Control and detection of chemical reactions in microfluidic systems. *Nature* **2006**, *442* (7101), 394–402.
- (4) Hartman, x. R. L.; Jensen, x. K. F. Microchemical systems for continuous-flow synthesis. *Lab Chip* **2009**, *9*, 2495–2507.
- (5) Hessel, V.; Lowe, H. Organic synthesis with microstructured reactors. *Chem. Eng. Technol.* **2005**, *28* (3), 267–284.
- (6) Jahnisch, K.; Hessel, V.; Lowe, H.; Baerns, M. Chemistry in microstructured reactors. *Angew. Chem., Int. Ed.* **2004**, *43* (4), 406–446.
- (7) Jensen, K. F. Microreaction engineering—is small better. *Chem. Eng. Sci.* **2001**, *56* (2), 293–303.
- (8) Jensen, K. F. Silicon-based microchemical systems: Characteristics and applications. *MRS Bull.* **2006**, *31* (2), 101–107.
- (9) Lee, C. C.; Sui, G. D.; Elizarov, A.; Shu, C. Y. J.; Shin, Y. S.; Dooley, A. N.; Huang, J.; Daridon, A.; Wyatt, P.; Stout, D.; Kolb, H. C.; Witte, O. N.; Satyamurthy, N.; Heath, J. R.; Phelps, M. E.; Quake, S. R.; Tseng, H. R. Multistep synthesis of a radiolabeled imaging probe using integrated microfluidics. *Science* **2005**, *310* (5755), 1793–1796.
- (10) Pennemann, H.; Watts, P.; Haswell, S. J.; Hessel, V.; Lowe, H. Benchmarking of microreactor applications. *Org. Process Res. Dev.* **2004**, *8* (3), 422–439.
- (11) Whitesides, G. M. The origins and the future of microfluidics. *Nature* **2006**, *442* (7101), 368–373.
- (12) Gunther, A.; Jensen, K. F. Multiphase microfluidics: from flow characteristics to chemical and materials synthesis. *Lab Chip* **2006**, *6* (12), 1487–1503.
- (13) Song, Y. J.; Hormes, J.; Kumar, C. Microfluidic synthesis of nanomaterials. *Small* **2008**, *4* (6), 698–711.
- (14) Hansen, C.; Quake, S. R. Microfluidics in structural biology: smaller, faster... better. *Curr. Opin. Struct. Biol.* **2003**, *13* (5), 538–544.
- (15) Trachsel, F.; Hutter, C.; von Rohr, P. R. Transparent silicon/glass microreactor for high-pressure and high-temperature reactions. *Chem. Eng. J.* **2008**, *135*, S309–S316.
- (16) Benito-Lopez, F.; Tiggelaar, R. M.; Salbut, K.; Huskens, J.; Egberink, R. J. M.; Reinhoudt, D. N.; Gardeniers, H.; Verboom, W. Substantial rate enhancements of the esterification reaction of phthalic anhydride with methanol at high pressure and using supercritical CO₂ as a co-solvent in a glass microreactor. *Lab Chip* **2007**, *7*, 1345–1351.
- (17) Verboom, W. Selected Examples of High-Pressure Reactions in Glass Microreactors. *Chem. Eng. Technol.* **2009**, *32* (11), 1695–1701.
- (18) Marre, S.; Park, J.; Rempel, J.; Guan, J.; Bawendi, M. G.; Jensen, K. F. Supercritical Continuous-Microflow Synthesis of Narrow Size Distribution Quantum Dots. *Adv. Mater.* **2008**, *20* (24), 4830.
- (19) Marre, S.; Aymonier, C.; Subra, P.; Mignard, E. Dripping to Jetting Transition observed from supercritical fluids in liquid microflows. *Appl. Phys. Lett.* **2009**, *95*, 134105.
- (20) Chambers, R. D.; Fox, M. A.; Sandford, G. Elemental fluorine - Part 18. Selective direct fluorination of 1,3-ketoesters and 1,3-diketones using gas/liquid microreactor technology. *Lab Chip* **2005**, *5* (10), 1132–1139.
- (21) Chambers, R. D.; Fox, M. A.; Sandford, G.; Trmcic, J.; Goeta, A. Elemental fluorine - Part 20. Direct fluorination of deactivated aromatic systems using microreactor techniques. *J. Fluorine Chem.* **2007**, *128* (1), 29–33.
- (22) de la Iglesia, O.; Sebastian, V.; Mallada, R.; Nikolaidis, G.; Coronas, J.; Kolb, G.; Zapf, R.; Hessel, V.; Santamaría, J. Preparation of Pt/ZSM-5 films on stainless steel microreactors. *Catal. Today* **2007**, *125* (1–2), 2–10.
- (23) Christian; Mitchell, M.; Kim, D. P.; Kenis, P. J. A. Ceramic microreactors for on-site hydrogen production. *J. Catal.* **2006**, *241* (2), 235–242.
- (24) Knitter, R.; Gohring, D.; Risthaus, P.; Hausselt, J. Microfabrication of ceramic microreactors. *Microsyst. Technol.* **2001**, *7* (3), 85–90.
- (25) Christian; Mitchell, M.; Kenis, P. J. A. Ceramic microreactors for on-site hydrogen production from high temperature steam reforming of propane. *Lab Chip* **2006**, *6* (10), 1328–1337.
- (26) Knitter, R.; Liauw, M. A. Ceramic microreactors for heterogeneously catalysed gas-phase reactions. *Lab Chip* **2004**, *4* (4), 378–383.
- (27) Jain, K.; Wu, C.; Atre, S. V.; Jovanovic, G.; Narayanan, V.; Kimura, S.; Sprenkle, V.; Canfield, N.; Roy, S. Synthesis of Nanoparticles in High Temperature Ceramic Microreactors: Design, Fabrication and Testing. *Int. J. Appl. Ceram. Technol.* **2009**, *6* (3), 410–419.

- (28) Kelley, S. C.; Deluga, G. A.; Smyrl, W. H. Miniature fuel cells fabricated on silicon substrates. *AIChE J.* **2002**, *48* (5), 1071–1082.
- (29) Sabate, N.; Esquivel, J. P.; Santander, J.; Torres, N.; Gracia, I.; Ivanov, P.; Fonseca, L.; Figueras, E.; Cane, C. Passive direct methanol fuel cells in silicon technology. *J. New Mater. Electrochem. Syst.* **2008**, *11* (2), 143–146.
- (30) Wu, X. H.; Guo, H.; Ye, F.; Ma, C. F. Application of Silicon in Micro Fuel Cells. *Prog. Chem.* **2009**, *21* (6), 1344–1348.
- (31) Iliescu, C.; Chen, B.; Miao, J. On the wet etching of Pyrex glass. *Sens. Actuators, A* **2008**, *143* (1), 154–161.
- (32) Tay, F. E. H.; Iliescu, C.; Jing, J.; Miao, J. M. Defect-free wet etching through pyrex glass using Cr/Au mask. *Microsyst. Technol.* **2006**, *12* (10–11), 935–939.
- (33) Mazurczyk, R.; El Khoury, G.; Dugas, V.; Hannes, B.; Laurenceau, E.; Cabrera, M.; Krawczyk, S.; Souteyrand, E.; Cloarec, J. P.; Chevrolat, Y. Low-cost, fast prototyping method of fabrication of the microreactor devices in soda-lime glass. *Sens. Actuators, B* **2008**, *128* (2), 552–559.
- (34) Zhu, J. J.; Cheng, J.; Ang, S. S.; Wang, H. Microfabrication of microfluidic channels on soda-lime glass. *Prog. Machin. Technol., Proc.* **2006**, *389*–392.
- (35) Tiggelaar, R. M.; Benito-Lopez, F.; Hermes, D. C.; Rathgen, H.; Egberink, R. J. M.; Mugele, F. G.; Reinholdt, D. N.; van den Berg, A.; Verboom, W.; Gardeniers, H. Fabrication, mechanical testing and application of high-pressure glass microreactor chips. *Chem. Eng. J.* **2007**, *131* (1–3), 163–170.
- (36) Murphy, E. R.; Inoue, T.; Sahoo, H. R.; Zaborenko, N.; Jensen, K. F. Solder-based chip-to-tube and chip-to-chip packaging for microfluidic devices. *Lab Chip* **2007**, *7*, 1309–1314.
- (37) Pattekar, A. V.; Kothare, M. V. Novel microfluidic interconnectors for high temperature and pressure applications. *J. Micromech. Microeng.* **2003**, *13* (2), 337–345.
- (38) Xiao, Z. X.; Wu, G. Y.; Li, Z. H.; Zhang, C. B.; Hao, Y. L.; Wang, Y. Y. Silicon-glass wafer bonding with silicon hydrophilic fusion bonding technology. *Sens. Actuators, A* **1999**, *72* (1), 46–48.
- (39) Schmidt, M. A. Wafer-to-wafer bonding for microstructure formation. *Proc. IEEE* **1998**, *86* (8), 1575–1585.
- (40) Sheu, J. T.; You, K. S.; Wu, C. H.; Chang, K. M. Optimization of KOH wet etching process in silicon nanofabrication. Proceedings of the 2001 1st IEEE Conference on Nanotechnology, 2001, pp 213–217.
- (41) Tokoro, K.; Uchikawa, D.; Shikida, M.; Sato, K. Anisotropic etching properties of silicon in KOH and TMAH solutions. MHS '98, Proceedings of the 1998 International Symposium on Micromechatronics and Human Science, 1998, pp 65–70.
- (42) Zubel, I. Silicon anisotropic etching in alkaline solutions. III. On the possibility of spatial structures forming in the course of Si(100) anisotropic etching in KOH and KOH plus IPA solutions. *Sens. Actuators, A* **2000**, *84* (1–2), 116–125.
- (43) Kim, B.; Cho, D. I. D. Aqueous KOH etching of silicon (110) - Etch characteristics and compensation methods for convex corners. *J. Electrochem. Soc.* **1998**, *145* (7), 2499–2508.
- (44) Sundaram, K. B.; Vijayakumar, A.; Subramanian, G. Smooth etching of silicon using TMAH and isopropyl alcohol for MEMS applications. *Microelectron. Eng.* **2005**, *77* (3–4), 230–241.
- (45) Aziz, N. A.; Bais, B.; Hamzah, A. A.; Majlis, B. Y. Characterization of HNA etchant for silicon microneedles array fabrication. *ICSE: 2008 IEEE Int. Conf. Semicond. Electron., Proc.* **2008**, 203–206.
- (46) Schwesinger, N.; Albrecht, A. Wet chemical isotropic etching procedures of silicon - a possibility for the production of deep structured microcomponents. *Micromachin. Microfab. Process Technol.* **1997**, *3223*, 72–79.
- (47) At every point in a stressed body there are at least three planes, called *principal planes*, with normal vectors **n**, called *principal directions*, where the corresponding stress vector is perpendicular to the plane, i.e., parallel or in the same direction as the normal vector **n**, and where there are no normal shear stresses τ_n . The three stresses normal to these principal planes are called *principal stresses*. (cf.⁴⁹ or any textbook on solid mechanics).
- (48) Rabier, J.; Demenet, J. L. Low temperature, high stress plastic deformation of semiconductors: The silicon case. *Phys. Status Solidi B* **2000**, *222* (1), 63–74.
- (49) Anderson, T. L. *Fracture Mechanics: Fundamentals and Applications*; Taylor & Francis Group: London, 1991.
- (50) Kurkjian, C. R.; Albarino, R. V.; Krause, J. T.; Vazirani, H. N.; Dimarcello, F. V.; Torza, S.; Schonhorin, H. Strength of 0.04–50-m lengths of coated fused silica fibers. *Appl. Phys. Lett.* **1976**, *28* (10), 588–590.
- (51) Sun, H. W.; Hill, T.; Schmidt, M.; Boning, D. Characterization and modeling of wafer and die level uniformity in deep reactive ion etching (DRIE). *Micro- and Nanosystems* **2004**, *782*, 435–440.
- (52) Yen, B. H. K. Microfluidic reactors for the synthesis of nanocrystals. Ph.D. Thesis, Massachusetts Institute of Technology, 2007.
- (53) Yen, B. K. H.; Gunther, A.; Schmidt, M. A.; Jensen, K. F.; Bawendi, M. G. A microfabricated gas-liquid segmented flow reactor for high-temperature synthesis: The case of CdSe quantum dots. *Angew. Chem., Int. Ed.* **2005**, *44* (34), 5447–5451.
- (54) Peles, Y.; Srikan, V. T.; Harrison, T. S.; Protz, C.; Mracek, A.; Spearing, S. M. Fluidic packaging of microengine and microrocket devices for high-pressure and high-temperature operation. *J. Microelectromech. Syst.* **2004**, *13* (1), 31–40.
- (55) Blom, M. T.; Chmela, E.; Gardeniers, J. G. E.; Berenschot, J. W.; Elwenspoek, M.; Tijsen, R.; van den Berg, A. Local anodic bonding of Kovar to Pyrex aimed at high-pressure, solvent-resistant microfluidic connections. *J. Micromech. Microeng.* **2001**, *11* (4), 382–385.
- (56) Nittis, V.; Fortt, R.; Legge, C. H.; de Mello, A. J. A high-pressure interconnect for chemical microsystem applications. *Lab Chip* **2001**, *1* (2), 148–152.
- (57) Muller, A.; Cominos, V.; Hessel, V.; Horn, B.; Schurer, J.; Ziogas, A.; Jahnisch, K.; Hillmann, V.; Grosser, V.; Jam, K. A.; Bazzanella, A.; Rinke, G.; Kraute, A. Fluidic bus system for chemical process engineering in the laboratory and for small-scale production. *Chem. Eng. J.* **2005**, *107* (1–3), 205–214.
- (58) Koch, C.; Ingle, J.; Remcho, V. Chips & Tips: Bonding Upchurch® NanoPorts to PDMS; http://www.rsc.org/Publishing/Journals/lc/Chips_and_Tips/nanoport_bonding.asp, 2008.
- (59) For more details on O-rings materials and groove design, please visit: <http://www.marcorubber.com/orings.htm>.
- (60) Young, W. C.; Budynas, R. G. *Roark's formulas for stress and strain*; McGraw-Hill: New York, 2002.
- (61) Broll, D.; Kaul, C.; Kramer, A.; Krammer, P.; Richter, T.; Jung, M.; Vogel, H.; Zehner, P. Chemistry in supercritical water. *Angew. Chem., Int. Ed.* **1999**, *38* (20), 2999–3014.
- (62) Loppinet-Serani, A.; Aymonier, C.; Cansell, F. Current and Foreseeable Applications of Supercritical Water for Energy and the Environment. *ChemSusChem* **2008**, *1* (6), 486–503.
- (63) Loppinet-Serani, A.; Aymonier, C.; Cansell, F. Supercritical Water for Environmental Technologies. *J. Chem. Technol. Biotechnol.* **2010**, *85*, 583–589.
- (64) Weingartner, H.; Franck, E. U. Supercritical water as a solvent. *Angew. Chem., Int. Ed.* **2005**, *44* (18), 2672–2692.
- (65) Brunner, G. Near and supercritical water. Part II: Oxidative processes. *J. Supercrit. Fluids* **2009**, *47* (3), 382–390.
- (66) Brunner, G. Near critical and supercritical water. Part I. Hydrolytic and hydrothermal processes. *J. Supercrit. Fluids* **2009**, *47* (3), 373–381.
- (67) Fraga-Dubreuil, J.; Poliakoff, M. Organic reactions in high-temperature and supercritical water. *Pure Appl. Chem.* **2006**, *78* (11), 1971–1982.
- (68) Ichishima, Y.; Hatakeyama, K.; Sato, O.; Yokoyama, T.; Arai, M. Acceleration of synthetic organic reactions using supercritical water: Noncatalytic Beckmann and pinacol rearrangements. *J. Am. Chem. Soc.* **2000**, *122* (9), 1908–1918.
- (69) Adschari, T. Supercritical hydrothermal synthesis of organic-inorganic hybrid nanoparticles. *Chem. Lett.* **2007**, *36*, 1188–1193.
- (70) Cansell, F.; Aymonier, C. Design of functional nanostructured materials using supercritical fluids. *J. Supercrit. Fluids* **2009**, *47* (3), 508–516.
- (71) Hall, J. B.; Jr.; Brewer, D. A. Supercritical Water Oxidation: Concept Analysis for Evolutionary Space Station Application, *16th International Conference on Environmental Systems*, SAE Technical Paper No. 860993, San Diego, CA, July 14–16, 1986.
- (72) The estimation of the residence time (t_R) was realized by taking into account the change in volumetric flow rates due to the fluid density variations between the HP/room temperature high pressure pump and the HT/HP operating conditions within the microreactor leading to $t_R = (\text{flow rate in pump/volume of microreactor})(\text{density hot area})/(\text{density in pump})$.
- (73) Krajnc, M.; Levec, J. On the kinetics of phenol oxidation in supercritical water. *AIChE J.* **1996**, *42* (7), 1977–1984.
- (74) Rice, S. F.; Hunter, T. B.; Ryden, A. C.; Hanush, R. G. Raman spectroscopic measurement of oxidation in supercritical water 0.1. Conversion of methanol to formaldehyde. *Ind. Eng. Chem. Res.* **1996**, *35* (7), 2161–2171.
- (75) Vogel, F.; Blanchard, J. L. D.; Marrone, P. A.; Rice, S. F.; Webley, P. A.; Peters, W. A.; Smith, K. A.; Tester, J. W. Critical review of kinetic data for the oxidation of methanol in supercritical water. *J. Supercrit. Fluids* **2005**, *34* (3), 249–286.
- (76) Park, J.; An, K. J.; Hwang, Y. S.; Park, J. G.; Noh, H. J.; Kim, J. Y.; Park, J. H.; Hwang, N. M.; Hyeon, T. Ultra-large-scale syntheses of monodisperse nanocrystals. *Nat. Mater.* **2004**, *3* (12), 891–895.

Received for review June 23, 2010
 Revised manuscript received September 14, 2010
 Accepted September 16, 2010

IE101346U